



Bihemispheric sensorimotor oscillatory network states determine cortical responses to transcranial magnetic stimulation

Yang Bai ^{a, b, c}, Paolo Belardinelli ^{a, b, d}, Ulf Ziemann ^{a, b, *}

^a Department of Neurology & Stroke, University of Tübingen, Tübingen, Germany

^b Hertie Institute for Clinical Brain Research, University of Tübingen, Tübingen, Germany

^c Center for Cognition and Brain Disorders, The Affiliated Hospital of Hangzhou Normal University, Hangzhou, China

^d Center for Mind/Brain Sciences - CIMEC, University of Trento, Italy

ARTICLE INFO

Article history:

Received 20 October 2021

Received in revised form

5 December 2021

Accepted 7 December 2021

Available online 8 December 2021

Keywords:

TMS-EEG

Bihemispheric oscillatory sensorimotor cortex states

Oscillatory power

Sensorimotor cortex

ABSTRACT

Background: Brain responses to external stimuli vary with fluctuating states of neuronal activity. Previous work has demonstrated effects of phase and power of the ongoing local sensorimotor μ -alpha-oscillation on responses to transcranial magnetic stimulation (TMS) of motor cortex (M1). However, M1 is part of a distributed network, and the effects of oscillatory activity in this network on TMS-evoked EEG responses (TEPs) have not been explored.

Objectives: To determine the effects of oscillatory activity in the bihemispheric sensorimotor network on TEPs.

Methods: 31 healthy subjects received single-pulse TMS of the left M1 hand area during EEG recording. Ongoing bihemispheric sensorimotor cortex oscillatory states were reconstructed from the EEG directly preceding TMS, and inferred by a data-driven method combining a multivariate autoregressive model and a Hidden Markov model. TEP amplitudes (P25, N45, P70, N100 and P180) were then compared between different bihemispheric sensorimotor cortex oscillatory states.

Results: Four bihemispheric sensorimotor cortex oscillatory states were identified, with different inter-hemispheric expressions of theta and alpha oscillations. High alpha-power states in the stimulated sensorimotor cortex increased P25 amplitude. Alpha power in the alpha-alpha state (stimulated - non-stimulated hemisphere) correlated in both hemispheres with N45 amplitude. Theta power in the alpha-theta state correlated in the non-stimulated hemisphere with P70 amplitude.

Conclusions: Bihemispheric sensorimotor cortex oscillatory states contribute to TEPs, with a relevance shift from stimulated to non-stimulated M1 from P25 over N45 to P70. This significantly extends previous findings: not only ongoing local oscillations but distributed network oscillatory states determine cortical responsiveness to external stimuli.

© 2021 The Authors. Published by Elsevier Inc. This is an open access article under the CC BY-NC-ND license (<http://creativecommons.org/licenses/by-nc-nd/4.0/>).

1. Introduction

The resting brain exhibits fluctuations of neuronal activity which are coordinated in space and time. The spontaneous fluctuations in human brain activity represent internal dynamics of neuronal activity and determine the response to external events, thereby contributing to the trial-to-trial variability in evoked brain responses [1]. Relevant interactions between spontaneous and task/stimulus-related neuronal activity have been reported in both

animal [2,3] and human brain [4,5]. In addition to narrowband oscillatory activity [6–8], broadband spontaneous neural activities contribute to brain states exhibiting dynamical multiregional coordination properties on a millisecond scale [9,10]. Such inherent transient states define spontaneous modes driven by oscillatory power, information flow and regional domination [11], and interact with task/stimulus-related neuronal activity [12–15].

Single-pulse transcranial magnetic stimulation (TMS) applied during electroencephalographic recordings (TMS-EEG) offers a unique possibility to directly probe the current brain state by linking the TMS-evoked potentials (TEPs) with excitability and connectivity of neuronal circuits. Supporting evidence for the interaction between ongoing brain states and TEPs comes from

* Corresponding author. Department of Neurology & Stroke, University of Tübingen, Hoppe-Seyler-Str. 3, 72076, Tübingen, Germany.

E-mail address: ulf.ziemann@uni-tuebingen.de (U. Ziemann).

studies comparing TEPs in particular brain states, such as in sleep [16] and anesthesia [17], or pathological conditions such as disorders of consciousness, stroke or attention deficit hyperactivity disorder [18–21]. However, TEPs are not only affected by overall alterations of brain states but also related to the continuously ongoing variation of neuronal activities. The cortical responses to TMS do not follow a rigid input-output function but are dynamically shaped by fluctuations of intrinsic neural properties at the time of stimulation [22]. Although high reproducibility of TEPs averaged over numerous trials (typically >100) has been reported in test-retest measurements [23], it is still largely unexplored how ongoing intrinsic fluctuations of brain state influence TEPs and contribute to their high inter-trial variability.

In primary motor cortex (M1), previous work has revealed distinct relationships between sensorimotor μ -rhythm phase and power with corticospinal excitability measured by motor evoked potentials (MEP) [24–27] and TEPs [28]. However, these studies focused on the μ -rhythm but have not addressed the potential role of other oscillations. Furthermore, M1 is not functionally segregated but dynamically integrated in extended sensorimotor networks [29,30]. Even ‘eyes closed’ and ‘eyes open’ conditions can affect motor responses to TMS [26]. In an integrative perspective, the spontaneous neural activities generated from the local cortices are organized into hierarchically nested specific global states [10,11,31]. Accordingly, we aimed at addressing to which extent activation and transition of intrinsic states in a bihemispheric sensorimotor network contribute to the expression of TEPs. To test this question, we used a novel data-driven method to disentangle the bihemispheric sensorimotor cortex states underlying spontaneous neural activity in the sensorimotor system. TEPs evoked by single-pulse TMS of left M1 were then analyzed with respect to these different bihemispheric sensorimotor states.

2. Methods

2.1. Participants

31 healthy male subjects (mean age \pm SD: 25.5 \pm 2.9 years, range: 21–36 years) took part in this study. All participants were screened for possible contraindications to TMS and met the criteria specified in the TMS safety screening questionnaire [32]. All subjects were right-handed according to the Edinburgh Handedness Inventory (laterality score $\geq 70\%$) [33]. Exclusion criteria included presence or history of neurologic and psychiatric disease, use of CNS active drugs, abuse of any drugs (including nicotine and alcohol). All participants gave informed written consent. The study was approved by the Ethics Committee of the Medical Faculty of the University of Tübingen.

2.2. Experimental set-up and data recording

Focal TMS of the hand area of left M1 was performed with a figure-of-eight coil (external diameter of each wing, 90 mm). The coil was connected with a Magstim 200² magnetic stimulator (Magstim Co, Whitland, Dyfed, UK) with a monophasic current waveform. Prior to TMS-EEG data recordings, individual resting motor threshold (RMT) and optimal coil position were determined by MEP recording from the right abductor pollicis brevis muscle (APB) muscle using surface EMG Ag–AgCl cup electrodes in a belly-tendon montage. The EMG raw signal was amplified and bandpass filtered (20 Hz–2 kHz; D360 amplifier, Digitimer) and digitized at an A/D rate of 10 kHz per channel (CED Micro 1401; Cambridge Electronic Design). Individual RMT was defined as the minimum intensity that was sufficient to elicit an MEP of > 50 peak-to-peak amplitude in at least five out of ten subsequent trials. The optimal

coil position was determined as the site that produced consistently the largest MEPs using a stimulation intensity slightly above RMT [34]. The optimal coil location was marked with a felt pen on the EEG cap to ensure consistent coil placement throughout the experiment. The coil orientation was set with the handle pointing backwards and 45° away from the midline. The induced current in the brain runs from lateral-posterior to medial-anterior, which is the optimal orientation for eliciting largest and most reliable MEPs [35].

Fifteen participants took part in three sessions (each session: 3 min resting-state EEG followed by 125 TMS pulses) and 16 participants took part in four sessions (each session: 3 min resting-state EEG followed by 150 TMS pulses) with the sessions in a given participant separated by at least 2 weeks. In each session, the participants were seated in a comfortable reclining chair and instructed to keep eyes open and to fixate a small black cross in front of them throughout the measurements. The participants were asked to wear earphones with white noise during the TMS-EEG recording to avoid EEG contamination by auditory evoked potentials caused by the TMS coil click [36]. The acoustic level of the white noise was calibrated until participants indicated that they could no longer hear the TMS clicks. RMT and optimal coil position were determined at the beginning of each measurement session. The resting-state EEG and TMS-EEG were recorded by a high-density EEG cap (EASYCAP GmbH, Germany) connected with a TMS-compatible EEG amplifier (BrainAmp DC, Brain Products GmbH, Munich, Germany). The EEG cap included 62 TMS-compatible C-ring slit EEG electrodes arranged in the International 10–20 montage with reference electrode at FCz. All electrode impedances were reduced (EEG gel: eci, Electro-Cap International Inc.; Abrasive gel: Nuprep, ADInstruments Ltd.) and maintained <5 k Ω throughout the measurements. The EEG amplifier was set with a 0.016–1000 Hz hardware filter and a 5 kHz sampling rate. During the TMS-EEG recordings, the single TMS pulses at an intensity of 100% RMT were delivered with a random interstimulus interval of 5 \pm 1 s [37,38].

2.3. Data processing

Processing of resting-state EEG datasets: Analyses were performed using customized analysis scripts on MATLAB R2017b and open source MATLAB toolboxes: EEGLAB 14.1.2b [39] and FieldTrip v20191014 [40]. The resting-state EEG data were band-pass filtered (1–40 Hz) and down-sampled to 200 Hz. Then, the data were segmented into epochs (8 s each, without overlap). Bad channels and epochs were identified and removed by combining Wiener estimation [41] and visual inspection. A FastICA algorithm-based independent components analysis (ICA) [42] was conducted on the retained epochs. Components were judged based on topography, weights in the epochs, and the spectrum to identify and remove eye blinks/movement and persistent muscle activity. Finally, the discarded channels were spline-interpolated using signal of the neighbor channels and data were then re-referenced to the average reference signal.

Processing of TMS-EEG datasets: The continuous TMS-EEG data were segmented into epochs with respect to the trigger markers. The epochs were defined from 500 ms before to 1 s after the marker. Baseline correction was performed based on average values between –500 ms and –5 ms of each epoch. Data from 1 ms before to 12 ms after the markers were excluded and cubic interpolated to eliminate the high-amplitude TMS artifact. EEG data were then visually inspected. Epochs containing major artifacts were identified and removed as well as channels that showed prominent noise in most of the epochs. The retained epochs were labeled according to the initial order to match with the EEG data preceding the TMS

pulses (see below). Afterwards, data was down-sampled to 1 kHz and submitted to a two-step ICA procedure, which has been recommended for TMS-EEG data processing [43]. In a first step, ICA components representing high-amplitude TMS related artifacts were inspected and removed based on the topography, single-trial time-course and average time-course. Then, data were filtered with a 1–100 Hz zero-phase Butterworth band-pass filter and a 48–52 Hz notch filter. As a second step, ICA was used to remove artifacts containing eye blinks, eye movement and persistent scalp muscle activity. Finally, the channels that were discarded during the visual inspection were spline-interpolated using signal of the neighbor channels and data were then re-referenced to the average reference signal.

Processing of EEG signals preceding the TMS pulses: The EEG data preceding the TMS pulses were selected by segmenting EEG data into epochs from 3.5 s to 2 ms before the TMS trigger markers. Zero-padding samples for 0.5 s were appended at the end of each epoch. Then, data were band-pass filtered (1–40 Hz) and down-sampled to 200 Hz. Afterwards, samples corresponding to 0.5 s after the beginning and 0.5 s before the end of each epoch were discarded to avoid edge distortion effects caused by the filtering. Bad channels and epochs with major artifacts were identified and removed by visual inspection. The retained epochs were labeled corresponding to initial order to match with TEPs. A FastICA algorithm was conducted. Components related to eye blinks/movement and persistent muscle activity were identified and removed. Finally, the discarded channels were spline-interpolated using signal of the neighbor channels and data were then re-referenced to the average reference signal. The retained post- and pre-TMS EEG epochs were matched and submitted to further analysis.

2.4. Source reconstruction

A template head model was constructed from the FreeSurfer fs_average MR image anatomy. A semi-automatic processing pipeline was performed with FieldTrip to segment the images into brain (2500 vertices), skull (2000 vertices), and scalp (1000 vertices) and to reconstruct the head model. A cortical mesh representing the midthickness surface between the grey and the white matter borders with 15684 dipole locations was considered as the source-space for EEG source localization. EEG electrodes were aligned to the template head model. The lead field matrix was calculated based on the aligned electrodes, cortical mesh, and head model. The conductivity was set as inside (0.33,0.004,0.33) and outside (0.004,0.33,0). Then, source reconstruction was performed using a linearly constrained minimum variance (LCMV) beamformer [44] according to the formulas defined by Sekihara [45].

2.5. Individual region of interests (ROIs)

In order to identify the bihemispheric sensorimotor cortex activities, we used individual source localization of the μ -rhythm to determine the sensorimotor regions of interest (ROIs) through the following steps (Fig. 1A): (i) Identify the individual μ -rhythm peak frequency by power spectral density (PSD) and topography within the range of 7–13 Hz. The individual μ -frequency band was defined as ± 1 Hz around the individual μ -rhythm peak frequency; (ii) Detect the time windows of μ -oscillation based on the individual μ -frequency band at the Hjorth-C3 and Hjorth-C4 electrode montages [24]. A power threshold (95th percentile of the theoretical probability distribution of power values at the μ -frequency band) and a duration threshold (6 complete cycles of individual μ -frequency band) were determined by subtracting a linear fit of colored noise spectrum from the wavelet power spectrum of each EEG channel (Hjorth-C3 and Hjorth-C4) [46]. Periods with relevant μ -rhythm

exceeded both the power and duration thresholds; (iii) Localize the source of the μ -oscillation power using the LCMV beamformer; (iv) Bootstrap sampling statistic to determine the significant dipoles at bihemispheric sensorimotor areas as ROIs. Oscillation power at source level was averaged in each time window. A bootstrap sampling method was used to shuffle 1000 times the dipole power values for each time window. The largest average values across all time windows were selected at each shuffling and the maximum distribution was used to assess thresholds for determining significant dipoles in each hemisphere with significance level at $p < 0.01$. The significant dipoles in each hemisphere were defined as ROI dipoles; (v) ROI activities were reconstructed from ROI dipoles. In each hemisphere, singular value decomposition (SVD) was conducted on the signals of ROI dipoles. The largest singular value and corresponding vector from SVD was used to reconstruct the ROI activity for each hemisphere. In this way, ROI activities were constructed from the EEG signal preceding the TMS pulse and the TEPs, to represent the bihemispheric sensorimotor activities before and after the TMS pulses.

2.6. Bi-hemispheric sensorimotor state inference and state features

Bihemispheric ROI activities from prior-to-TMS time windows were submitted to a state inference procedure [9]. The state inference combined two well-known models: the multivariate autoregressive model (MAR) [47] and the Hidden Markov model (HMM) [48]. The MAR model provided the description characteristics representing linear historical interactions between the signals from the bihemispheric ROIs. For each time t , the MAR model predicted the bihemispheric ROI signal values as a linear combination of signal values at $[t - 1, t - 2, \dots, t - P]$. In this way, both the autocorrelation structure of the signal and interactions between bihemispheric ROIs were characterized. The parameter P defines how many previous time points are used to predict each time point. It is crucial to optimize the order parameter P , to have sufficient samples for data prediction and avoid model over-fitting at the same time. According to the free-energy based parameter selection strategy [9,12], we used free-energy to monitor the convergence of the model computation aiming to minimize the cost in variational inference. In this study, the parameter $P = 4$ represented the optimal trade-off between predictability and parsimony (Supplementary Information Fig. S3). Lower P -values correspond to lower free-energy but P values ≤ 3 cannot disentangle the inherent states and result in repetitive invalid states driven by same oscillation group.

An HMM was used to describe the time series as a sequence of states, where each state includes its own MAR description. For each time point, HMM estimates states according to the probabilities of being at a given state predicted by MAR, and probability of being at a given state depends on the state's assignment in the previous time point. Then, the state time-courses (Fig. 1B) with state activation probabilities, and a Viterbi path, defined as the most likely sequence of states, were estimated by a variation Bayes inference [9,31,49]. The number of states (K) represents one further crucial parameter in the state inference. This should be specified before the model inference, depending on how many activated states were hypothesized in the investigated data. In this study, the μ -power values of bihemispheric sensorimotor areas ($n = 2$) were used to motivate the state expression and transition. In practice, the model was inferred using $K = 2, 3, \dots, 6$. Although higher state numbers ($K > 4$) provided for a more fine-grained solution, some less-informative states, which were dominated by few or even a single subject, were driven by individual outliers but not general oscillations (Supplementary Information Fig. S4). The number of states $K = 4$ showed moderately lower free-energy, higher state

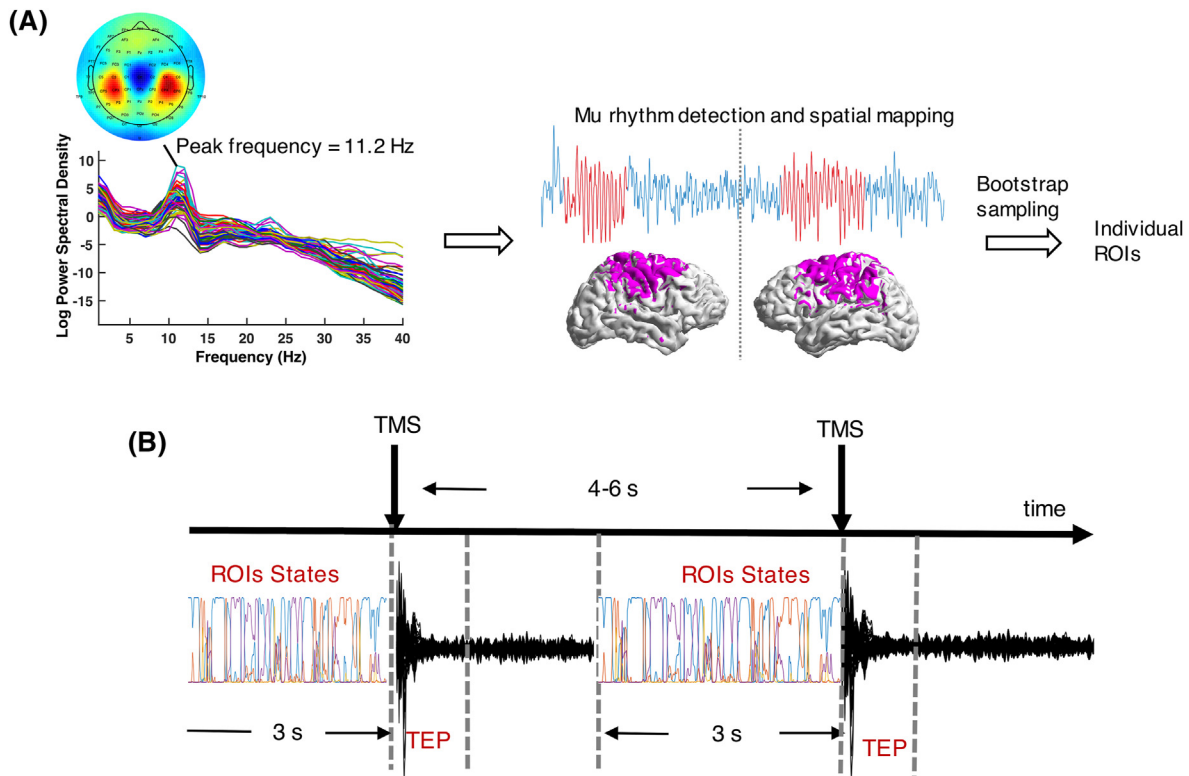


Figure 1. Schematic description of the pipeline for the selection of individual regions of interest (ROI) and computation of ROI state-dependent TMS evoked potentials (TEPs). (A) Spectral power and topography of resting-state EEG were used to select the individual μ -rhythm peak frequency. An oscillation detection procedure based on the μ -rhythm individual peak frequency was run to determine the time windows with relevant μ -rhythm. Band-pass filtered signals in μ -rhythm time windows were mapped in the source space. A bootstrap sampling statistics approach was applied on the dipole power values to determine the individual ROI dipoles in both hemispheres. (B) Bihemispheric ROI activities within 3 s time windows before the TMS pulses were constructed from ROI dipoles and submitted to a state inference procedure based on a combination of a multivariate autoregressive model and a Hidden Markov model. The state expression time courses were generated with the relative probabilities of state activation at each time point. The relationship between TEPs and the activated states at the time of TMS pulse was then investigated.

resolution with respect to lower values and without effects from individual difference. We hence chose $K = 4$ for state inference in this study. The same parameters ($K = 4$, $P = 4$) were used to infer the states of bihemispheric ROI activities from pure resting-state EEG (i.e., without TMS) in order to cross-validate these states and parameters.

A parametric model estimation was performed based on the MAR state coefficients to represent the underlying oscillations which drive the state expression [9]. On the other hand, we conducted a nonparametric PSD estimation based on the multitaper approach to measure the real spectrum of the prior-to-TMS activities identified by the states [49,50]. These PSDs describe spectral characteristic of the states' activities across all the activation time windows. Furthermore, the state activation sequence of each participant was described using three types of temporal features: fractional occupancy, life time, and interval time. The fractional occupancy refers to the total time spent by the participant in each state. The life time and interval time refer to the duration of each state's activation and the interval between two visits of a given state, respectively.

2.7. Statistical analysis

For each temporal feature (fractional occupancy, life time, interval time), a one-way repeated measure analysis of variance (rmANOVA) with the effect of state (4 levels: state 1–4) was performed, and post-hoc paired-sample t -tests were performed in case of a significant effect of state to compare the states with each other.

P values after multiple comparisons were adjusted using Bonferroni correction.

To investigate the relationship between the bihemispheric sensorimotor states and TEPs, all TEP epochs that matched prior-to-TMS epochs were identified by state (state 1–4) with respect to the activation state at the time of the TMS pulse. The PSD of the prior-to-TMS activities with respect to each state was measured and compared between the different states by a two-way rmANOVA with the effect of states (4 levels: state 1–4) and hemispheres (2 levels: left and right). P values of the post-hoc t -tests were adjusted for multiple comparisons using the Bonferroni correction.

The state comparison analysis of TEPs was conducted in source space. We conducted singular value decomposition on the TEPs of individual ROI dipoles after source reconstruction. The vector corresponding to the largest principle component represented the sensorimotor source TEP (ROI-TEP). The TEPs were averaged within each subject. Five non-overlapping times of interest (TOIs) were considered [51,52]: P25 (25–35 ms), N45 (40–50 ms), P70 (55–70 ms), N100 (90–125 ms) and P180 (160–200 ms) to cover major TEP components observed with M1 stimulation [53,54]. Firstly, a two-way rmANOVA was performed with effects of states (4 levels: state 1–4) and TOIs (5 levels: P25, N45, P70, N100 and P180). Then, the TEP amplitudes in each TOI were compared between the different state conditions using one-way rmANOVAs, and Bonferroni correction was applied to correct p values of the post-hoc t -tests for multiple comparisons. Relationships between TEP amplitude and oscillatory power/fractional occupancy were checked by Pearson correlation analyses and simple linear

regressions with scatter-plots. Significance level was set as $P < 0.05$ for all statistical analyses. In order to highlight the differences specified by the alpha-alpha and alpha-theta states, we compared the state dependent TEPs vs. the average of all other states and considered the difference of state dependent oscillatory power values (a specific state vs. the average of all other states) for correlation analysis. The Pearson correlation was measured firstly at each dipole and then between the average TEPs across all significant dipoles of each subject and oscillatory power. In addition, we measured the correlation between the average TEPs of individual ROI dipoles and oscillatory power.

3. Results

3.1. Bihemispheric sensorimotor oscillatory network states

The ROI definition procedure performed effectively: the significant common ROI dipoles obtained by bootstrap sampling among all subjects showed a distribution map on bihemispheric sensorimotor areas (Supplementary Information Fig. S2). Individual ROI selections are reported in Supplementary Information Fig. S1.

Four sensorimotor oscillatory network states were inferred from model analysis, driven by specific oscillatory activities and interactions of the bihemispheric sensorimotor regions. They are referred to as alpha-theta state (state 1), theta-theta state (state 2), theta-alpha state (state 3) and alpha-alpha state (state 4) according to the parametric model estimation (Fig. 2A). Specifically, the alpha-theta state (state 1) was distinctly driven by inherent activities of alpha in the stimulated left sensorimotor cortex, and theta in the non-stimulated right sensorimotor cortex. The theta-alpha

state (state 3) was a reversal of state 1, i.e., theta in the left sensorimotor cortex and alpha in the right sensorimotor cortex. The theta-theta (state 2) and alpha-alpha states (state 4) were driven by bihemispheric theta and alpha activities, respectively. The PSDs of bihemispheric activities defined by the states showed high peaks of alpha activity in the stimulated left sensorimotor cortex in the alpha-theta and alpha-alpha states, and high peaks of alpha activity in the non-stimulated right sensorimotor cortex in the theta-alpha and alpha-alpha states (Fig. 2B). These states were clearly reproducible when we conducted the state inference in the ROI activities of resting-state EEG with the same parameters (Supplementary Information Fig. S7A).

The temporal properties of the states were characterized from the state expression sequence. The fractional occupancy was significantly different between states ($F_{(1.57, 46.95)} = 21.75$, $p < 0.001$) while all states were represented in every subject (Fig. 2C). Alpha-theta and theta-theta states occupied significantly more ($p < 0.001$ after Bonferroni correction) time than the theta-alpha and alpha-alpha states. The life time analysis denoted that all states were short lived with mean values between 50 and 100 ms and showed significant differences between the states ($F_{(1.44, 43.13)} = 39.11$, $p < 0.001$, Fig. 2D). The alpha-theta state showed significantly longer life times (mean \pm 1SD, 90.1 ± 20.1 ms, $p < 0.001$) and shorter intervals until onset of the next identical state (mean \pm 1SD, 0.28 ± 0.08 s, $p < 0.001$, Fig. 2E) compared to all other states. These results were confirmed by the temporal features of the states achieved in the cross-validation analysis from the resting-state EEG data (Supplementary Information Figs. S7B–D).

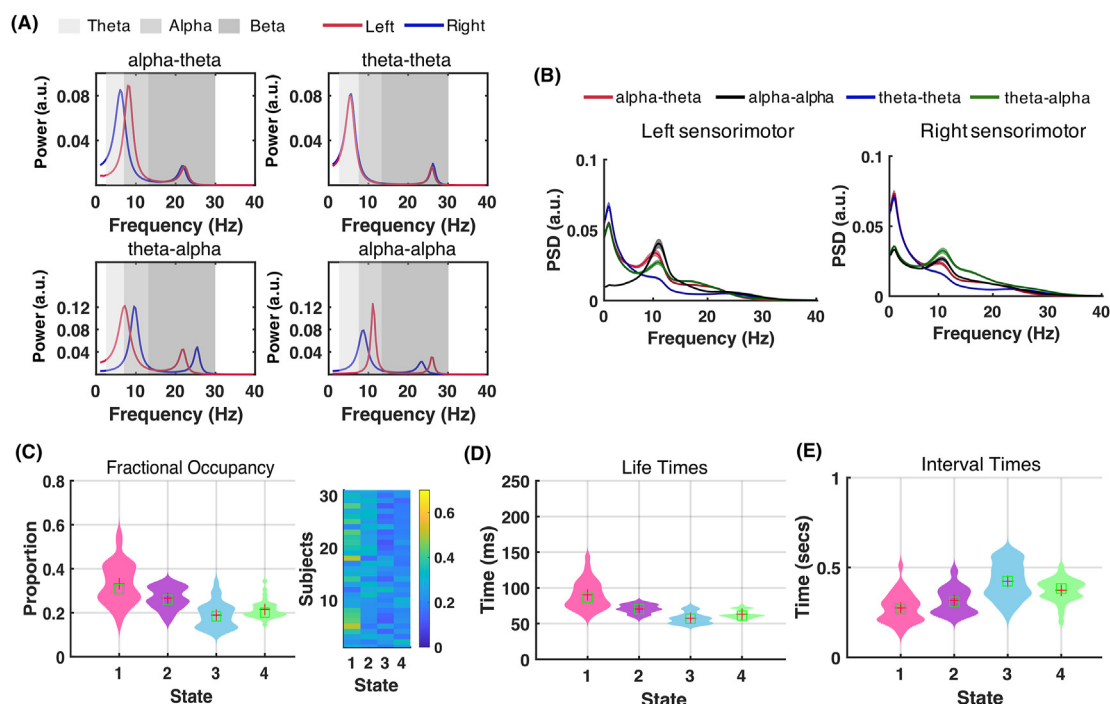


Fig. 2. States estimated by model inference. (A) Parametric model estimation (power in arbitrary units, a.u.) of the four states (red: stimulated left sensorimotor cortex, blue: non-stimulated right sensorimotor cortex), which are referred to as: alpha-theta state (state 1), theta-theta state (state 2), theta-alpha state (state 3), and alpha-alpha state (state 4). The theta, alpha and beta frequency bands are indicated by different shades of grey. (B) Power spectral densities (mean \pm 1SD, in arbitrary units, a.u.) of the bihemispheric ROI activities in the four states (indicated by different colors). Distribution plots were used to show the fractional occupancy (C), life times (D) and intervals to the next identical state (E) for each of the states. Red crosses and green squares show the mean and median values, respectively, in each distribution. Panel right of fractional occupancy plot shows fractional occupancy distribution in each of the individual 31 subjects. (For interpretation of the references to color in this figure legend, the reader is referred to the Web version of this article.)

3.2. Alpha power in the stimulated left sensorimotor cortex modulates the P25 TEP

Average TEPs at sensor level and topography plots of defined TOIs are shown in Supplementary Information (Fig. S10). In total, 3224 trials were identified as alpha-theta state TEPs, 1758 trials as theta-theta state TEPs, 1980 trials as theta-alpha state TEPs, and 1984 trials as alpha-alpha state TEPs. The trial numbers in individual subjects in each state as well as state-specific average TEPs across subjects are provided in Supplementary Information (Fig. S11). Subsequently, we divided the TEPs into high alpha-power (H-alpha) and low alpha-power (L-alpha) groups according to the states at the time of the TMS pulse. In practice, TEPs identified by the alpha-theta and alpha-alpha states were classified as H-alpha according to the distinct characteristic of alpha oscillation in the stimulated left sensorimotor cortex in the PSD of these states. Accordingly, TEPs identified by theta-alpha state and theta-theta state were classified as L-alpha. The states showed a significant effect on PSDs of prior-to-TMS activities ($F_{(2.07, 124.38)} = 176.87$, $p < 0.001$), and a significant interaction with regions ($F_{(2.07, 124.38)} = 54.85$, $p < 0.001$). In the stimulated left sensorimotor cortex, H-alpha group showed significantly higher alpha power than L-alpha group ($F_{(1, 60)} = 56.67$, $p < 0.001$, Fig. 3A), while no difference was observed in the PSDs in the non-stimulated right sensorimotor cortex (Fig. 3B). Comparisons of TEPs between H-alpha and L-alpha groups were conducted at source space (Fig. 3C–D). After reconstruction of sensorimotor responses from

individual ROI dipoles (Fig. S1 in Supplementary Information), we found a significantly higher P25 amplitude ($F_{(1, 30)} = 12.26$, $p = 0.001$) in the H-alpha (0.194 ± 0.285 , mean \pm 1SD) vs. L-alpha group (0.090 ± 0.153) (Fig. 3C–D). The TEPs in the other TOIs did not show any significant difference for the H-alpha vs. L-alpha comparison (Fig. S5 in Supplementary Information).

There was no significant correlation between P25 amplitudes and alpha power, neither in the stimulated left sensorimotor cortex ($r = 0.173$, $p > 0.05$) nor in the non-stimulated right sensorimotor cortex ($r = 0.368$, $p > 0.05$) (Fig. 4A). However, the fractional occupancy of the H-alpha states significantly correlated ($r = 0.393$, $p = 0.03$) with the P25 amplitudes at group level (Fig. 4B). Fig. 4C shows the correlations between the P25 amplitudes of dipoles and the fractional occupancy of the H-alpha states. The dipoles displaying a significant correlation of P25 amplitude with fractional occupancy in the H-alpha states were mainly distributed in the pre- and post-central gyrus of the stimulated left hemisphere (Fig. 4C, Fig. S12A in Supplementary Information shows the dipoles in an inflated brain). Average P25 amplitude values of the significant dipoles showed a positive correlation with the fractional occupancy of the H-alpha states ($r = 0.667$, $p < 0.001$) (Fig. 4D).

3.3. Alpha and theta power in the non-stimulated right sensorimotor cortex modulate the N45 and P70 TEPs

We compared TEPs in source space between each particular state vs. the average of all other states. The prior-to-TMS activities

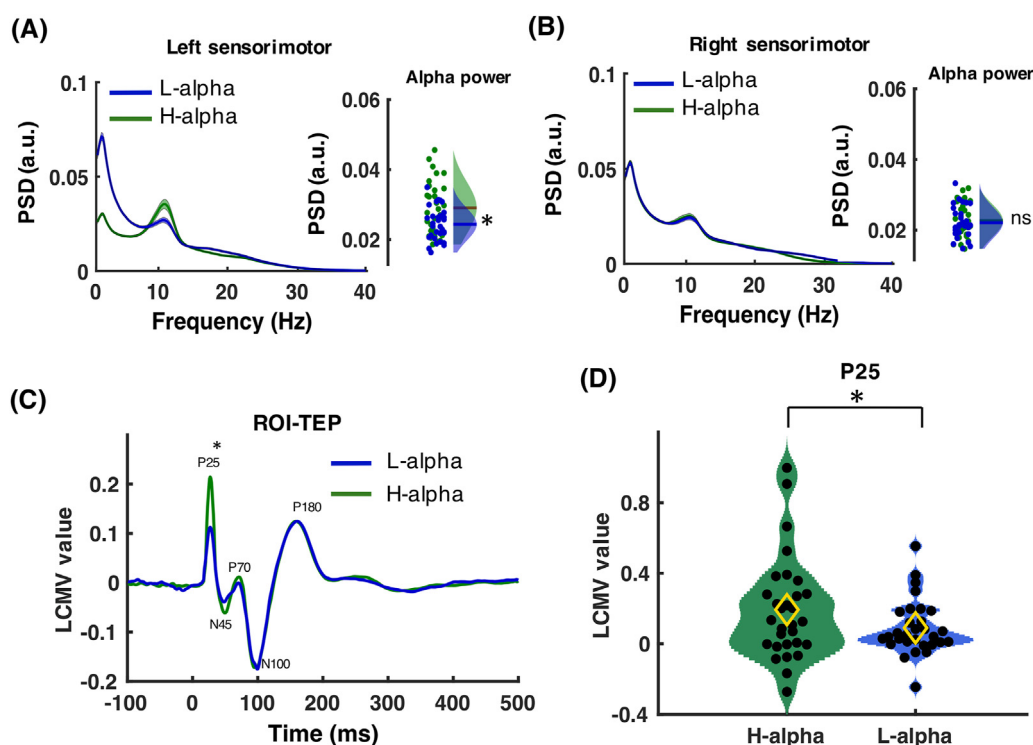


Fig. 3. Power spectral densities (PSD, in arbitrary units, a.u.) of prior-to-TMS activities and corresponding source space TMS evoked potentials (TEPs) in high alpha-power (H-alpha) and low alpha-power (L-alpha) groups. PSDs were measured by a multitaper approach on prior-to-TMS activities in the stimulated left sensorimotor cortex (A) and the non-stimulated right sensorimotor cortex (B). Right panels show alpha powers of all participants and corresponding Gaussian distributions in the H-alpha (green) and L-alpha (blue) conditions. Asterisk indicates significance in two-way rmANOVA with post-hoc *t*-tests after Bonferroni correction, ns means non-significance. (C) The sensorimotor TEPs (ROI-TEP) were reconstructed by the largest principle component of the TEPs of individual ROI dipoles (cf. Fig. S1 in Supplementary Information) and expressed by the linearly constrained minimum variance (LCMV) value. The TEPs were averaged in H-alpha (green) and L-alpha (blue) groups across all subjects ($n = 31$). Five time windows of interest (TOIs) were defined: P25 (25–35 ms), N45 (40–50 ms), P70 (55–70 ms), N100 (90–125 ms) and P180 (160–200 ms). The distribution plot (D) shows P25 amplitude of all subjects at H-alpha and L-alpha groups. Black dots represent values of individual subjects, with yellow diamonds showing the means. The asterisk denotes a significant difference between P25 amplitudes in H-alpha vs. L-alpha group (one-way rmANOVA with post-hoc *t*-tests after Bonferroni correction). Fig. S5 in Supplementary Information shows the distribution plots of the other TOIs (N45, P70, N100 and P180). (For interpretation of the references to color in this figure legend, the reader is referred to the Web version of this article.)

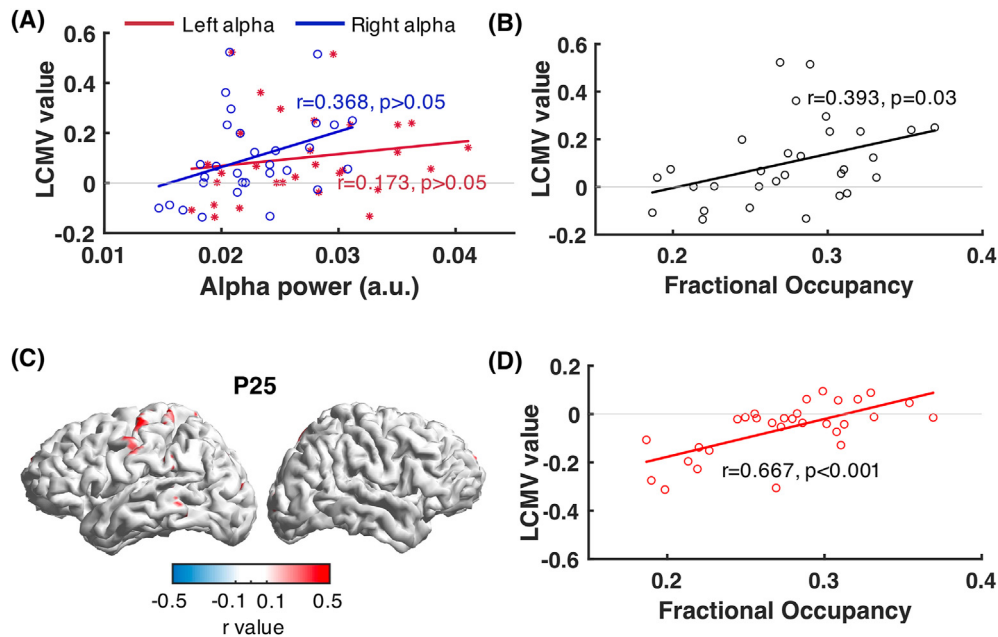


Fig. 4. Pearson correlations between P25 amplitudes of individual ROI dipoles (cf. Fig. S1 in Supplementary Information) and expressed by the linearly constrained minimum variance (LCMV) value vs. oscillatory power or fractional occupancy of prior-to-TMS states. Scatter plots of P25 amplitudes related to alpha power in the stimulated left sensorimotor cortex (A, red), alpha power in the non-stimulated right sensorimotor cortex (A, blue), and fractional occupancy of H-alpha states (B). (C) Spatial distribution of the dipoles which showed significant correlation ($p < 0.05$) between P25 amplitudes and fractional occupancy in the H-alpha power states. Plots in the inflated brain are given in Supplementary Information (Fig. S12A). (D) Scatter plots and Pearson correlation between average P25 amplitudes across all significant dipoles and fractional occupancy of H-alpha-power states. Each circle or asterisk represents data of one subject. Regression lines and Pearson correlations with correlation coefficients (r) and p values are indicated. Color bar shows r value of Pearson correlation. Red and blue color indicate positive and negative correlation, respectively. (For interpretation of the references to color in this figure legend, the reader is referred to the Web version of this article.)

showed significantly higher alpha power in the alpha-alpha vs. the average of all other states in both sensorimotor cortices (Left: $F_{(1, 30)} = 91.55, p < 0.001$; Right: $F_{(1, 30)} = 32.07, p < 0.001$, Fig. 5A–B). The reconstructed left sensorimotor cortex TEPs (ROI-TEP) in the alpha-alpha state showed significantly higher P25 (i.e., more positive; $F_{(1, 30)} = 8.62, p = 0.006$; 0.137 ± 0.185 vs. 0.099 ± 0.154) and N45 peaks (i.e., more negative; $F_{(1, 30)} = 12.92, p = 0.001$; -0.072 ± 0.132 vs. -0.024 ± 0.112) than the average of all other states (Fig. 5C and D). There were no significant differences at P70, N100 and P180 (Fig. S6A in Supplementary Information). When comparing the alpha-theta state with the average of all other states, the prior-to-TMS activities showed significantly higher alpha power in the stimulated left sensorimotor cortex ($F_{(1, 30)} = 105.19, p < 0.001$) and higher theta power ($F_{(1, 30)} = 77.72, p < 0.001$) at the non-stimulated right sensorimotor cortex (Fig. 7A–B). Accordingly, the alpha-theta state showed a significantly increased P25 ($F_{(1, 30)} = 10.08, p = 0.003$; 0.146 ± 0.211 vs. 0.100 ± 0.149) and P70 ($F_{(1, 30)} = 10.20, p = 0.003$; 0.019 ± 0.104 vs. -0.022 ± 0.101) peak (i.e., more positive, Fig. 7C–D). There were no significant differences for N45, N100 and P180 (Fig. S6B in Supplementary Information).

Then, we investigated the relationships between the state-dependent TEP amplitudes and oscillatory power in each condition. In the alpha-alpha state, there existed dipoles (mainly located in the bihemispheric sensorimotor cortex) showing significant inverse correlation between the N45 amplitudes with the alpha power (difference between alpha-alpha state and average across all other states) of the stimulated left sensorimotor cortex ($r = -0.364, p = 0.045$) (Fig. 6A–B) and non-stimulated right sensorimotor cortex ($r = -0.373, p = 0.042$) (Fig. 6C–D). In other words, higher alpha power at the bihemispheric sensorimotor cortices corresponded to more negative N45 amplitudes (i.e., a higher N45 peak) in these dipoles (Fig. S12C in Supplementary Information shows the dipoles in an inflated brain). When constrained to the subjects'

sensorimotor cortex, the N45 amplitudes of the stimulated left hemisphere (average of individual ROI dipoles shown in Fig. S1 in Supplementary Information) still showed inverse correlation with the alpha power (difference with the average across all other states) of the stimulated left sensorimotor cortex ($r = -0.435, p = 0.016$) and non-stimulated right sensorimotor cortex ($r = -0.475, p = 0.008$) (Fig. 6E).

In the alpha-theta state, the P70 amplitudes in the stimulated left sensorimotor cortex (average of individual ROI dipoles shown in Fig. S1 in Supplementary Information) did not show a significant correlation with the difference values of alpha power (difference with the average of all other states) in the stimulated left sensorimotor cortex ($r = 0.168, p > 0.05$), but a direct correlation with theta power (difference with the average of all other states) in the contralateral right sensorimotor cortex ($r = 0.390, p = 0.032$) (Fig. 8A). In other words, the higher theta power in the non-stimulated right sensorimotor cortex corresponded to higher P70 amplitudes in the stimulated left sensorimotor cortex. The significant dipoles with a positive correlation of P70 amplitude and theta power ($r = 0.448, p = 0.013$) were not only located in the region of the bilateral sensorimotor cortices but also in bilateral frontal regions (Fig. 8B–C, Fig. S12B in Supplementary Information shows the dipoles in an inflated brain).

4. Discussion

Previous studies from our group revealed effects of the interaction between sensorimotor μ -alpha rhythm phase and power, and TMS readouts of motor cortical excitability [24,25,27,28], but the extent to which the TEPs are influenced by ongoing fluctuations of sensorimotor cortical networks is still largely unknown. Previous studies did not consider the continuously fluctuating brain dynamics at broadband and did not address the effects of spatially

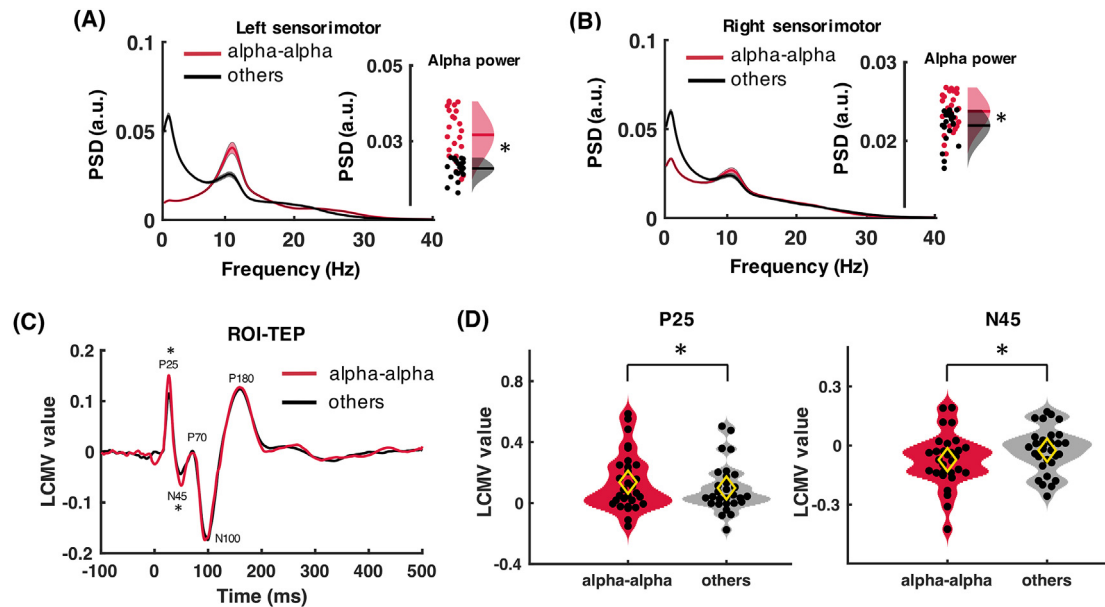


Fig. 5. Power spectral densities (PSD, in arbitrary units, a.u.) of prior-to-TMS activities and corresponding source space TMS evoked potentials (TEPs) in the alpha-alpha state vs. average of all other states. PSDs were measured by a multitaper approach on prior-to-TMS activities in the stimulated left sensorimotor cortex (A) and non-stimulated right sensorimotor cortex (B). Panels right to the PSD plots show alpha powers of all subjects and corresponding Gaussian distributions in the alpha-alpha state (red) and average of all other states (black). Asterisks indicate significance in two-way rmANOVA with post-hoc *t*-tests after Bonferroni correction. (C) The left sensorimotor TEPs (ROI-TEP) were reconstructed by the largest principle component of the TEPs of individual ROI dipoles (cf. Fig. S1 in Supplementary Information) and expressed by the linearly constrained minimum variance (LCMV) value. The TEPs were averaged in alpha-alpha state (red) and average of all other states (black) across all subjects ($n = 31$). The distribution plots (D) show amplitudes in times of interest (P25 and N45) of all subjects in the alpha-alpha state vs. average of all other states. Black dots represent values of individual subjects, with yellow diamonds showing the means. The asterisks denote a significant difference between alpha-alpha state vs. average of all other states (one-way rmANOVA with post-hoc *t*-tests after Bonferroni correction). Fig. S6A in Supplementary Information shows the distribution plots of the other times of interest (P70, N100 and P180). (For interpretation of the references to color in this figure legend, the reader is referred to the Web version of this article.)

extended sensorimotor network interactions on TEPs. We report here bihemispheric sensorimotor EEG consisting of the dynamical expression and transition (at millisecond scale) of oscillatory network states, representing oscillatory integrative patterns of interhemispheric sensorimotor activity. These spontaneously occurring states could be identified through a completely data-

driven analysis pipeline, which takes autocorrelations and cross-correlations within multiple brain regions into account for state inference. The main novel finding of this work is that the spontaneous expression of these states prior to TMS pulses to the left M1 contributes significantly to the modulation TEP amplitudes. We found that oscillatory activities in the sensorimotor regions of both

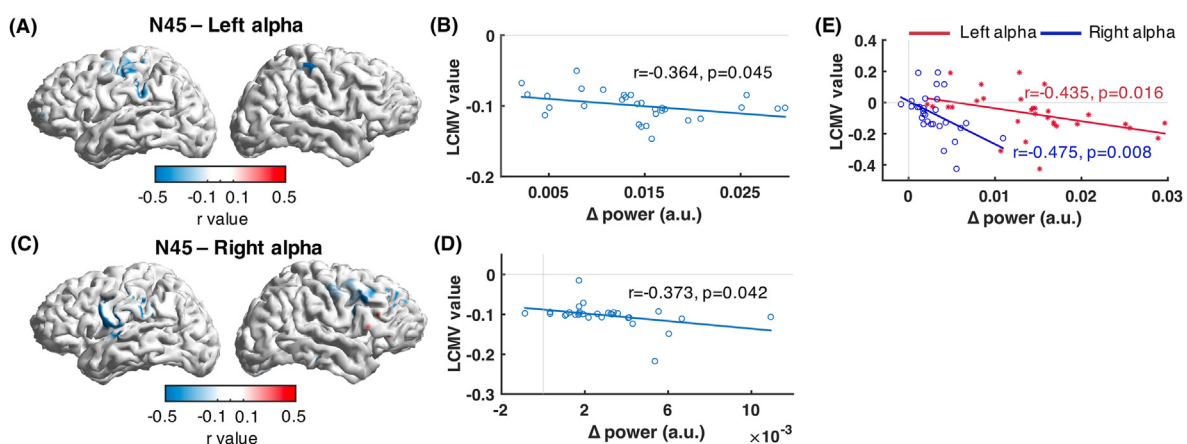


Fig. 6. Pearson correlations between N45 amplitudes in the alpha-alpha state of individual ROI dipoles (cf. Fig. S1 in Supplementary Information) and expressed by the linearly constrained minimum variance (LCMV) value vs. alpha power of prior-to-TMS states. Spatial distribution plots show dipoles with significant correlation between N45 amplitudes in the alpha-alpha state and alpha power (difference between alpha-alpha state and average across all other states) in the stimulated left sensorimotor cortex (A) and in the non-stimulated right sensorimotor cortex (C). Plots in the inflated brain are given in Supplementary Information (Fig. S12C). Color bar shows *r* value of Pearson correlation. Red and blue color indicate positive and negative correlations, respectively. Scatter plots and Pearson correlations between average N45 amplitudes across all significant dipoles and relative alpha power in the stimulated left sensorimotor cortex are shown in (B), and in the non-stimulated right sensorimotor cortex in (D). (E) Scatter plots and Pearson correlations of N45 amplitudes of alpha-alpha state in stimulated left sensorimotor cortex (cf. Fig. S1 in Supplementary Information for the individual dipoles) as a function of the difference values of alpha power of the alpha-alpha state vs. the average of all other states in the stimulated left sensorimotor cortex (red) and in the non-stimulated right sensorimotor cortex (blue). Regression lines and Pearson correlations with correlation coefficients and *p* values are indicated. (For interpretation of the references to color in this figure legend, the reader is referred to the Web version of this article.)

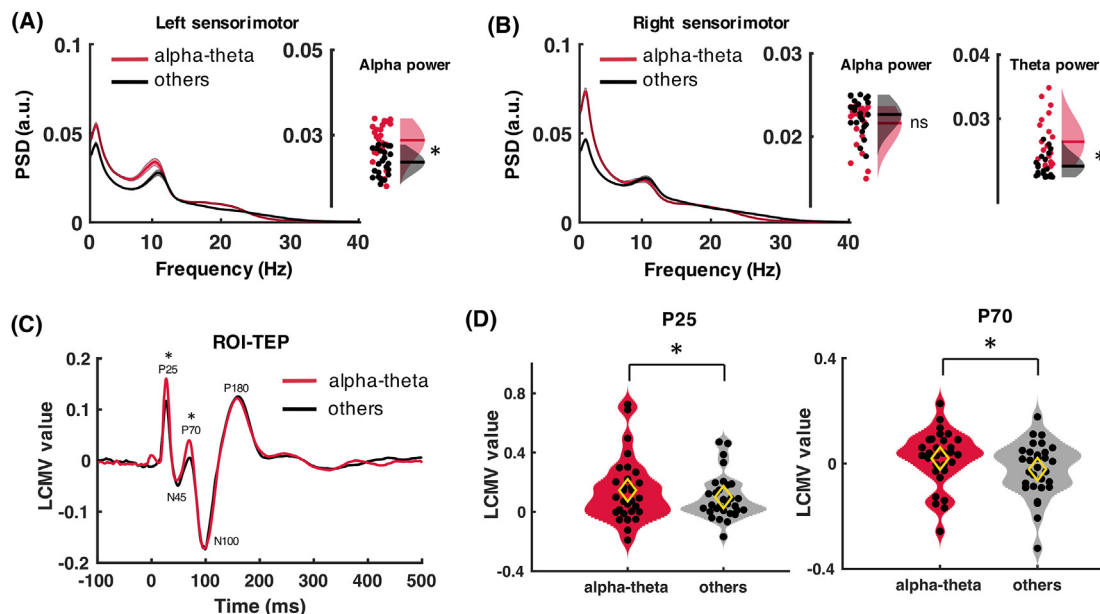


Fig. 7. Power spectral densities (PSD, in arbitrary units, a.u.) of prior-to-TMS activities and corresponding source space TMS evoked potentials (TEPs) in the alpha-theta state vs. average of other states. PSDs were measured by a multitaper approach on prior-to-TMS activities in the stimulated left sensorimotor cortex (A) and the non-stimulated right sensorimotor cortex (B). Panels right to the PSD plots show alpha powers of the subjects and corresponding Gaussian distributions in the alpha-theta (red) and average of other states (black). Asterisks indicate significance in two-way rmANOVA with post-hoc *t*-tests after Bonferroni correction. (C) The left sensorimotor TEPs (ROI-TEP) were reconstructed by the largest principle component of the TEPs of individual ROI dipoles (cf. Fig. S1 in Supplementary Information) and expressed by the linearly constrained minimum variance (LCMV) value. The TEPs were averaged in alpha-theta state (red) and average of other states (black) across all subjects ($n = 31$). The distribution plots (D) show amplitudes in times of interest (P25 and P70) of all subjects in the alpha-theta state and average of other states. Black dots represent values of individual subjects, with yellow diamonds showing the means. The asterisks denote a significant difference between alpha-theta state vs. average of other states (one-way rmANOVA with post-hoc *t*-tests after Bonferroni correction). Fig. S6B in Supplementary Information shows the distribution plots of the other times of interest (N45, N100 and P180). (For interpretation of the references to color in this figure legend, the reader is referred to the Web version of this article.)

the stimulated left and non-stimulated right sensorimotor cortex modulate TEPs in different time windows. Our results link the sensorimotor TEP amplitudes with fluctuating oscillatory integrative patterns of the bihemispheric sensorimotor network.

4.1. Bi-hemispheric sensorimotor oscillatory network states

The states were inferred from the reconstructed spontaneous neural activities in the bihemispheric sensorimotor oscillatory network through data-driven analysis. The methodology has been proven reliable in modeling brain activity as a dynamic sequence of distinct brain network states in both task and rest conditions [9,12,31]. Each state in this study exhibits a specific bihemispheric oscillatory integration pattern. In general, theta and alpha

oscillations were highlighted in driving the state expression in the bihemispheric sensorimotor system. Although the roles of theta and μ -alpha oscillations in sensorimotor cortex have been elucidated to some extent [55–57], the states obtained in this study essentially revealed a new approach of 'coupling' in the bihemispheric sensorimotor system. Differently from previous studies focused on connectivity measures derived from oscillatory activity [58,59], the oscillatory network states were distinctly driven by the power, autocorrelation and cross-correlation of an oscillation in the stimulated left sensorimotor cortex and in the non-stimulated right sensorimotor cortex. Moreover, state transitions represent the dynamic fluctuations in the bihemispheric sensorimotor network at a 50–100 ms time scale. Additionally, the obtained states, representing the interaction of distributed cortical networks through

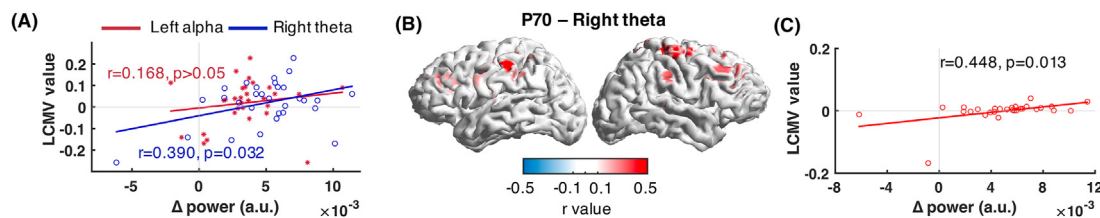


Fig. 8. Pearson correlations between P70 amplitudes in alpha-theta state of individual ROI dipoles (cf. Fig. S1 in Supplementary Information) and expressed by the linearly constrained minimum variance (LCMV) value vs. oscillation power in prior-to-TMS states. (A) Scatter plots and Pearson correlations of P70 amplitudes in the alpha-theta state in the stimulated left sensorimotor cortex as a function of the difference values (between alpha-theta state and average of all other states) of alpha power in the stimulated left sensorimotor cortex (red), and of theta power in the non-stimulated right sensorimotor cortex (blue). Each circle or asterisk represents the data of one subject. Regression lines and Pearson correlations with correlation coefficients (*r*) and *p* values are indicated. (B) Spatial distribution of dipoles with significant correlation between P70 amplitude in the alpha-theta state and theta power (difference between alpha-theta state and average across all other states) in the non-stimulated right sensorimotor. Plots in the inflated brain are given in the Supplementary Information (Fig. S12B). Color bar shows *r* value of Pearson correlation. Red and blue color indicate positive and negative correlations, respectively. Right panel (C) shows scatter plot and Pearson correlation between average P70 amplitudes across all significant dipoles and relative theta power in the non-stimulated right sensorimotor cortex. (For interpretation of the references to color in this figure legend, the reader is referred to the Web version of this article.)

oscillatory 'coupling' could be considered as evidence for the theory of communication through coherence [60]. Interhemispheric oscillatory synchronization (by 20–40 Hz oscillations) has been defined in the sensorimotor cortex during bimanual and unimanual motor tasks [61]. The states obtained in this study extend the bihemispheric synchronization of sensorimotor cortices to resting state.

One of the critical questions when applying the state inference is whether the states were driven by general properties across all subjects or dominated by outliers. The fractional occupancy map provides the percentage of signals that can be explained as a specific state expression. Despite differences in some individuals, the states maintained a distinct and consistent expression in all subjects. Less-informative states, without evident oscillatory information, tended to be driven by outliers when we mandatorily set a larger state number for inference (Supplementary Information Fig. S4). We provide evidence that the observed states in this study captured the group commonalities and gave an optimal resolution in oscillatory information disaggregation. Furthermore, a cross-validation was conducted by comparing states which were obtained by separate inference with the same model parameters, from the data sets of prior-to-TMS EEG epochs and resting-state EEG. The consistent driving oscillations and temporal distribution (Supplementary Information Fig. S7) provide evidence that these states were reproducible in the bihemispheric sensorimotor network irrespective of TMS. Another question that needs clarification regards the potential cumulative effects of TMS pulses on cortical excitability or neurodynamics [62,63]. We counted the number of state expressions along with the number of TMS pulses in each measurement and each subject. All state expressions appeared robust throughout the measurements (Supplementary Information Fig. S9). Moreover, the consistent temporal distributions of the states when comparing the data sets of prior-to-TMS epochs and resting-state EEG also indicated that the overall state expressions in prior-to-TMS epochs were not significantly affected by possible cumulative TMS effects.

4.2. Endogenous oscillations modulate TEPs on bihemispheric sensorimotor states

Previous studies have demonstrated that MEP amplitude as a marker of corticospinal excitability is associated with the power of the ongoing μ -alpha rhythm [25,27,64,65]. However, at variance to these studies on the effects of ongoing neural oscillations derived from a single site (i.e., the stimulated sensorimotor cortex) on MEP amplitudes, our study focused on the bihemispheric sensorimotor network. This is of interest as neural activities in the motor cortices of the two hemispheres interact, mainly through the corpus callosum [30,66–68], and this interaction is important for motor behavior such as intermanual coordination [69]. The results of this study provide evidence that oscillatory network states integrated across both hemispheres influence sensorimotor TEPs. The results essentially revealed an interaction between the instantaneously ongoing theta and μ -alpha oscillations in the sensorimotor cortices of both hemispheres and the cortical response to TMS.

Both high alpha-power states in the left sensorimotor cortex (alpha-alpha state and alpha-theta state) modulated the P25 amplitude in the stimulated left sensorimotor cortex (Figs. 3D, 5D and 7D). P25 amplitude reflects corticospinal excitability of the stimulated motor cortex [52,70]. The expression of the high alpha-power states included most part of the individual μ -alpha rhythm activation in the stimulated left sensorimotor cortex, as they occupied over 60% of the time of μ -rhythm activation (Supplementary Information Fig. S8). Therefore, the present findings are consistent with the previously demonstrated direct

relation of MEP amplitude with μ -alpha power [25–27,65]. Neuronal assemblies in the brain oscillate and thereby undergo rhythmic fluctuations of excitation and inhibition [71]. The states driven by oscillations in this study essentially represent a series of neuronal oscillatory models. Therefore, the relationship between cortical excitability (P25 amplitude) and the ongoing states suggests that state expression and transition might be physiologically caused by the fluctuations of excitation and inhibition of neurons. Additionally, the modulation of P25 amplitude by state suggests that the dynamical state expression in a given subject contributes to the high inter-trial variability of TEPs. However, at group level, the individual P25 amplitude did not show a direct correlation with the individual μ -alpha power but significantly correlated with the fractional occupancy of high alpha power states (Fig. 4).

Beside modulation of P25 amplitude, the bihemispheric sensorimotor oscillatory states also demonstrated state-specific modulation of later TEPs (N45 and P70). The N45 peak was significantly increased in the alpha-alpha state, while the P70 peak was significantly increased in the alpha-theta state. Moreover, the present results provide evidence that the cortical excitability (identified by the alpha-power) in the stimulated sensorimotor cortex is not the sole contributor to N45 and P70 amplitudes, as both alpha-alpha and alpha-theta state are associated with high P25 amplitude and represent high alpha-power in the stimulated left sensorimotor cortex but had distinct selective modulatory effects on N45 and P70 amplitude (Figs. 5D and 7D). The significant correlations between the TEP amplitudes and oscillatory power in the non-stimulated right sensorimotor cortex revealed that the non-stimulated contralateral sensorimotor cortex was involved in the modulation of N45 and P70 peaks (Figs. 6E and 8C). Taking into account the close relationship between μ -alpha power and motor excitability, the results indicate that the N45 peak in the alpha-alpha state is co-regulated by bilateral motor excitability [26]. On the contrary, the P70 peak was primarily modulated by theta power in the non-stimulated sensorimotor cortex and specific to the alpha-theta state, as a dominant contralateral theta in the theta-theta state did not show effects on P70 amplitude.

In summary, our results imply that the impact of μ -alpha power in the stimulated sensorimotor cortex on TEPs shows a gradual decrease from early to later TEP components ($P25 > N45 > P70 > N100$), while the impact of oscillatory power in the non-stimulated sensorimotor cortex shows a gradual increase ($P25 < N45 < P70$). Therefore, the results reveal that bihemispheric sensorimotor oscillatory network states determine cortical TEPs. The TEP components were not solely dependent on ongoing sensorimotor oscillations at the site of stimulation but also on ongoing oscillations in the non-stimulated contralateral hemisphere. Taking into account bihemispheric brain states may have major implications for the implementation of individualized and brain-state-dependent TMS-EEG approaches to render brain responses to TMS more robust and reliable.

5. Limitations

The number of states for model inference was determined in a practical way based on a strategy, balancing oscillatory decomposing resolution and inconsistency due to individual difference. Our results do not imply that only these 4 states exist in the bihemispheric sensorimotor integrated activity. Since our approach is completely data driven, the state numbers and state content only depend on the signal itself and are easily affected by signal-to-noise ratio and outliers. This was addressed here by demonstrating that strong outliers were not existent, and by cross-validation in two separate model inferences of different recordings (prior-to-TMS EEG and resting-state EEG). Higher resolution of state inference

might have been achieved by other neuroimaging techniques such as magnetoencephalography and individual MRIs for source reconstruction. Finally, since we investigated cortical responses to TMS of sensorimotor cortex, potential somatosensory-evoked potential (SEP), induced by direct excitation of trigeminal afferents or MEP-related afferent feedback, may have confounded our results. Conflicting findings from previous investigations [72–74] render the relevance of contamination of early TEPs (<100 ms) by SEPs somewhat inconclusive, but future experiments with realistic sham stimulation protocols including stimulation of peripheral nerves could validate the present findings further [75].

CRedit authorship contribution statement

Yang Bai: Conceptualization, Data collection, Formal analysis, Writing – original draft, Final approval of the version to be published. **Paolo Belardinelli:** Formal analysis, Writing – original draft, Final approval of the version to be published. **Ulf Ziemann:** Conceptualization, Formal analysis, Critical revision of the article, Final approval of the version to be published.

Declaration of competing interest

The authors declare that they have no known competing financial interests or personal relationships that could have appeared to influence the work reported in this paper.

Acknowledgement

This work was supported by the National Natural Science Foundation of China (61901155); Medicine and Health Science and Technology Project of Zhejiang Province (2019RC254); and the Alexander-von-Humboldt foundation (3.5–1203399 - CHN - HFST-P).

Appendix A. Supplementary data

Supplementary data to this article can be found online at <https://doi.org/10.1016/j.brs.2021.12.002>.

References

- [1] Sadaghiani S, Hesselmann G, Friston KJ, Kleinschmidt A. The relation of ongoing brain activity, evoked neural responses, and cognition. *Front Syst Neurosci* 2010;4:20.
- [2] Arieli A, Sterkin A, Grinvald A, Aertsen A. Dynamics of ongoing activity: explanation of the large variability in evoked cortical responses. *Science* 1996;273(5283):1868–71.
- [3] Azouz R, Gray CM. Cellular mechanisms contributing to response variability of cortical neurons in vivo. *J Neurosci* 1999;19(6):2209–23.
- [4] Fox MD, Snyder AZ, Zacks JM, Raichle ME. Coherent spontaneous activity accounts for trial-to-trial variability in human evoked brain responses. *Nat Neurosci* 2006;9(1):23–5.
- [5] Fox MD, Snyder AZ, Vincent JL, Raichle ME. Intrinsic fluctuations within cortical systems account for intertrial variability in human behavior. *Neuron* 2007;56(1):171–84.
- [6] Thut G, Nietzel A, Brandt SA, Pascual-Leone A. Alpha-band electroencephalographic activity over occipital cortex indexes visuospatial attention bias and predicts visual target detection. *J Neurosci* 2006;26(37):9494–502.
- [7] van Dijk H, Schoffelen JM, Oostenveld R, Jensen O. Prestimulus oscillatory activity in the alpha band predicts visual discrimination ability. *J Neurosci* 2008;28(8):1816–23.
- [8] van Ede F, de Lange F, Jensen O, Maris E. Orienting attention to an upcoming tactile event involves a spatially and temporally specific modulation of sensorimotor alpha- and beta-band oscillations. *J Neurosci* 2011;31(6):2016–24.
- [9] Vidaurre D, Quinn AJ, Baker AP, Dupret D, Tejero-Cantero A, Woolrich MW. Spectrally resolved fast transient brain states in electrophysiological data. *Neuroimage* 2016;126:81–95.
- [10] Vidaurre D, Smith SM, Woolrich MW. Brain network dynamics are hierarchically organized in time. *Proc Natl Acad Sci U S A* 2017;114(48):12827–32.
- [11] Vidaurre D, Hunt LT, Quinn AJ, Hunt BA, Brookes MJ, Nobre AC, et al. Spontaneous cortical activity transiently organises into frequency specific phase-coupling networks. *Nat Commun* 2018;9(1):1–13.
- [12] Vidaurre D, Abeyurriya R, Becker R, Quinn AJ, Alfaro-Almagro F, Smith SM, et al. Discovering dynamic brain networks from big data in rest and task. *Neuroimage* 2018;180(Pt B):646–56.
- [13] Cabral J, Vidaurre D, Marques P, Magalhães R, Moreira PS, Soares JM, et al. Cognitive performance in healthy older adults relates to spontaneous switching between states of functional connectivity during rest. *Sci Rep* 2017;7(1):1–13.
- [14] Quinn AJ, Vidaurre D, Abeyurriya R, Becker R, Nobre AC, Woolrich MW. Task-evoked dynamic network analysis through hidden markov modeling. *Front Neurosci* 2018;12:603.
- [15] Vidaurre D, Myers NE, Stokes M, Nobre AC, Woolrich MW. Temporally unconstrained decoding reveals consistent but time-varying stages of stimulus processing. *Cerebr Cortex* 2019;29(2):863–74.
- [16] Massimini M, Ferrarelli F, Huber R, Esser SK, Singh H, Tononi G. Breakdown of cortical effective connectivity during sleep. *Science* 2005;309(5744):2228–32.
- [17] Ferrarelli F, Massimini M, Sarasso S, Casali A, Riedner BA, Angelini G, et al. Breakdown in cortical effective connectivity during midazolam-induced loss of consciousness. *Proc Natl Acad Sci U S A* 2010;107(6):2681–6.
- [18] Casali AG, Gosseries O, Rosanova M, Boly M, Sarasso S, Casali KR, et al. A theoretically based index of consciousness independent of sensory processing and behavior. *Sci Transl Med* 2013;5(198):198ra05.
- [19] Rosanova M, Gosseries O, Casarotto S, Boly M, Casali AG, Bruno MA, et al. Recovery of cortical effective connectivity and recovery of consciousness in vegetative patients. *Brain* 2012;135(Pt 4):1308–20.
- [20] Bruckmann S, Hauk D, Roessner V, Resch F, Freitag CM, Kammer T, et al. Cortical inhibition in attention deficit hyperactivity disorder: new insights from the electroencephalographic response to transcranial magnetic stimulation. *Brain* 2012;135(Pt 7):2215–30.
- [21] Tscherpel C, Dern S, Hensel L, Ziemann U, Fink GR, Grefkes C. Brain responsiveness provides an individual readout for motor recovery after stroke. *Brain* 2020;143(6):1873–88.
- [22] Bergmann TO, Molle M, Schmidt MA, Lindner C, Marshall L, Born J, et al. EEG-guided transcranial magnetic stimulation reveals rapid shifts in motor cortical excitability during the human sleep slow oscillation. *J Neurosci* 2012;32(1):243–53.
- [23] Lioumis P, Kicic D, Savolainen P, Makela JP, Kahkonen S. Reproducibility of TMS-Evoked EEG responses. *Hum Brain Mapp* 2009;30(4):1387–96.
- [24] Zrenner C, Desideri D, Belardinelli P, Ziemann U. Real-time EEG-defined excitability states determine efficacy of TMS-induced plasticity in human motor cortex. *Brain Stimul* 2018;11(2):374–89.
- [25] Thies M, Zrenner C, Ziemann U, Bergmann TO. Sensorimotor mu-alpha power is positively related to corticospinal excitability. *Brain Stimul* 2018;11(5):1119–22.
- [26] Ogata K, Nakazono H, Uehara T, Tobimatsu S. Prestimulus cortical EEG oscillations can predict the excitability of the primary motor cortex. *Brain Stimul* 2019;12(6):1508–16.
- [27] Bergmann TO, Lieb A, Zrenner C, Ziemann U. Pulsed facilitation of corticospinal excitability by the sensorimotor mu-alpha rhythm. *J Neurosci* 2019;39(50):10034–43.
- [28] Desideri D, Zrenner C, Ziemann U, Belardinelli P. Phase of sensorimotor mu-oscillation modulates cortical responses to transcranial magnetic stimulation of the human motor cortex. *J Physiol* 2019;597(23):5671–86.
- [29] Serrien DJ, Ivry RB, Swinnen SP. Dynamics of hemispheric specialization and integration in the context of motor control. *Nat Rev Neurosci* 2006;7(2):160–6.
- [30] Stefanou M-I, Desideri D, Belardinelli P, Zrenner C, Ziemann U. Phase synchrony of μ -rhythm determines efficacy of interhemispheric communication between human motor cortices. *J Neurosci* 2018;38(49):10525–34.
- [31] Baker AP, Brookes MJ, Rezek IA, Smith SM, Behrens T, Probert Smith PJ, et al. Fast transient networks in spontaneous human brain activity. *Elife* 2014;3:e01867.
- [32] Rossi S, Antal A, Bestmann S, Bikson M, Brewer C, Brockmüller J, et al. Safety and recommendations for TMS use in healthy subjects and patient populations, with updates on training, ethical and regulatory issues: expert guidelines. 2020.
- [33] Oldfield RC. The assessment and analysis of handedness: the Edinburgh inventory. *Neuropsychologia* 1971;9(1):97–113.
- [34] Groppa S, Oliviero A, Eisen A, Quartarone A, Cohen LG, Mall V, et al. A practical guide to diagnostic transcranial magnetic stimulation: report of an IFCN committee. *Clin Neurophysiol* 2012;123(5):858–82.
- [35] Di Lazzaro V, Ziemann U, Lemon RN. State of the art: physiology of transcranial motor cortex stimulation. *Brain Stimul* 2008;1(4):345–62.
- [36] Nikouline V, Ruohonen J, Ilmoniemi RJ. The role of the coil click in TMS assessed with simultaneous EEG. *Clin Neurophysiol* 1999;110(8):1325–8.
- [37] Premoli I, Castellanos N, Rivolta D, Belardinelli P, Bajo R, Zipser C, et al. TMS-EEG signatures of GABAergic neurotransmission in the human cortex. *J Neurosci* 2014;34(16):5603–12.
- [38] Belardinelli P, König F, Liang C, Premoli I, Desideri D, Müller-Dahlhaus F, et al. TMS-EEG signatures of glutamatergic neurotransmission in human cortex. *Sci Rep* 2021;11(1):8159.

- [39] Delorme A, Makeig S. EEGLAB: an open source toolbox for analysis of single-trial EEG dynamics including independent component analysis. *J Neurosci Methods* 2004;134(1):9–21.
- [40] Oostenveld R, Fries P, Maris E, Schoffelen JM. FieldTrip: open source software for advanced analysis of MEG, EEG, and invasive electrophysiological data. *2011 Comput Intell Neurosci* 2011;156869.
- [41] Mutanen TP, Metsomaa J, Liljander S, Ilmoniemi RJ. Automatic and robust noise suppression in EEG and MEG: the SOUND algorithm. *Neuroimage* 2018;166:135–51.
- [42] Hyvarinen A, Oja E. Independent component analysis: algorithms and applications. *Neural Network* 2000;13(4–5):411–30.
- [43] Rogasch NC, Thomson RH, Farzan F, Fitzgibbon BM, Bailey NW, Hernandez-Pavon JC, et al. Removing artefacts from TMS-EEG recordings using independent component analysis: importance for assessing prefrontal and motor cortex network properties. *Neuroimage* 2014;101:425–39.
- [44] Van Veen BD, van Drongelen W, Yuchtman M, Suzuki A. Localization of brain electrical activity via linearly constrained minimum variance spatial filtering. *IEEE Trans Biomed Eng* 1997;44(9):867–80.
- [45] Sekihara K, Nagarajan SS. Adaptive spatial filters for electromagnetic brain imaging. Springer Science & Business Media; 2008.
- [46] Whitten TA, Hughes AM, Dickson CT, Caplan JB. A better oscillation detection method robustly extracts EEG rhythms across brain state changes: the human alpha rhythm as a test case. *Neuroimage* 2011;54(2):860–74.
- [47] Penny W, Roberts S. Bayesian multivariate autoregressive models with structured priors. *IEEE Proc Vis Image Signal Process* 2002;149(1):33–41.
- [48] Juang B-H, Rabiner L. Mixture autoregressive hidden Markov models for speech signals. *IEEE Trans Acoust Speech Signal Process* 1985;33(6):1404–13.
- [49] Vidaurre D, Hunt LT, Quinn AJ, Hunt BAE, Brookes MJ, Nobre AC, et al. Spontaneous cortical activity transiently organises into frequency specific phase-coupling networks. *Nat Commun* 2018;9(1):2987.
- [50] Jachan M, Henschel K, Nawrath J, Schad A, Timmer J, Schelter B. Inferring direct directed-information flow from multivariate nonlinear time series. *Phys Rev E - Stat Nonlinear Soft Matter Phys* 2009;80(1 Pt 1):011138.
- [51] Komssi S, Kahkonen S, Ilmoniemi RJ. The effect of stimulus intensity on brain responses evoked by transcranial magnetic stimulation. *Hum Brain Mapp* 2004;21(3):154–64.
- [52] Ahn S, Frohlich F. Pinging the brain with transcranial magnetic stimulation reveals cortical reactivity in time and space. *Brain Stimul* 2021;14(2):304–15.
- [53] Ilmoniemi RJ, Kicic D. Methodology for combined TMS and EEG. *Brain Topogr* 2010;22(4):233–48.
- [54] Tremblay S, Rogasch NC, Premoli I, Blumberger DM, Casarotto S, Chen R, et al. Clinical utility and prospective of TMS-EEG. *Clin Neurophysiol* 2019;130(5):802–44.
- [55] Kay LM. Theta oscillations and sensorimotor performance. *Proc Natl Acad Sci U S A* 2005;102(10):3863–8.
- [56] Cruikshank LC, Singhal A, Hueppelsheuser M, Caplan JB. Theta oscillations reflect a putative neural mechanism for human sensorimotor integration. *J Neurophysiol* 2012;107(1):65–77.
- [57] Haegens S, Nacher V, Luna R, Romo R, Jensen O. alpha-Oscillations in the monkey sensorimotor network influence discrimination performance by rhythmical inhibition of neuronal spiking. *Proc Natl Acad Sci U S A* 2011;108(48):19377–82.
- [58] Fries P. Rhythms for cognition: communication through coherence. *Neuron* 2015;88(1):220–35.
- [59] Canolty RT, Knight RT. The functional role of cross-frequency coupling. *Trends Cognit Sci* 2010;14(11):506–15.
- [60] Fries P. A mechanism for cognitive dynamics: neuronal communication through neuronal coherence. *Trends Cognit Sci* 2005;9(10):474–80.
- [61] Murthy VN, Fetz EE. Oscillatory activity in sensorimotor cortex of awake monkeys: synchronization of local field potentials and relation to behavior. *J Neurophysiol* 1996;76(6):3949–67.
- [62] Stamoulis C, Oberman LM, Praeg E, Bashir S, Pascual-Leone A. Single pulse TMS-induced modulations of resting brain neurodynamics encoded in EEG phase. *Brain Topogr* 2011;24(2):105–13.
- [63] Pellicciari MC, Miniussi C, Ferrari C, Koch G, Bortoletto M. Ongoing cumulative effects of single TMS pulses on corticospinal excitability: an intra- and inter-block investigation. *Clin Neurophysiol* 2016;127(1):621–8.
- [64] Hussain SJ, Claudino L, Bonstrup M, Norato G, Cruciani G, Thompson R, et al. Sensorimotor oscillatory phase-power interaction gates resting human corticospinal output. *Cerebr Cortex* 2019;29(9):3766–77.
- [65] Karabanov AN, Madsen KH, Krohne LG, Siebner HR. Does pericentral mu-rhythm “power” corticomotor excitability?—A matter of EEG perspective. *Brain Stimul* 2021;14(3):713–22.
- [66] Ferbert A, Priori A, Rothwell JC, Day BL, Colebatch JG, Marsden CD. Inter-hemispheric inhibition of the human motor cortex. *J Physiol* 1992;453:525–46.
- [67] Ugawa Y, Hanajima R, Kanazawa I. Interhemispheric facilitation of the hand area of the human motor cortex. *Neurosci Lett* 1993;160(2):153–5.
- [68] Wahl M, Lauterbach-Soon B, Hattungen E, Jung P, Singer O, Volz S, et al. Human motor corpus callosum: topography, somatotopy, and link between micro-structure and function. *J Neurosci* 2007;27(45):12132–8.
- [69] Swinnen SP. Intermanual coordination: from behavioural principles to neural-network interactions. *Nat Rev Neurosci* 2002;3(5):348–59.
- [70] Mäki H, Ilmoniemi RJ. The relationship between peripheral and early cortical activation induced by transcranial magnetic stimulation. *Neurosci Lett* 2010;478(1):24–8.
- [71] Buzsaki G, Draguhn A. Neuronal oscillations in cortical networks. *Science* 2004;304(5679):1926–9.
- [72] Gordon PC, Desideri D, Belardinelli P, Zrenner C, Ziemann U. Comparison of cortical EEG responses to realistic sham versus real TMS of human motor cortex. *Brain Stimul* 2018;11(6):1322–30.
- [73] Conde V, Tomasevic L, Akopian I, Stanek K, Saturnino GB, Thielscher A, et al. The non-transcranial TMS-evoked potential is an inherent source of ambiguity in TMS-EEG studies. *Neuroimage* 2019;185:300–12.
- [74] Rocchi L, Di Santo A, Brown K, Ibáñez J, Casula E, Rawji V, et al. Disentangling EEG responses to TMS due to cortical and peripheral activations. *Brain stim* 2021;14(1):4–18.
- [75] Gordon PC, Jovellar DB, Song Y, Zrenner C, Belardinelli P, Siebner HR, et al. Recording brain responses to TMS of primary motor cortex by EEG - utility of an optimized sham procedure. *Neuroimage* 2021;118708.